journal

J. Am. Ceram. Soc., 96 [2] 391–397 (2013)
DOI: 10.1111/jace.12126

Ceramic Capillary Suspensions: Novel Processing Route for Macroporous Ceramic Materials

Jens Dittmann,† Erin Koos, and Norbert Willenbacher

Karlsruhe Institute of Technology, Institute for Mechanical Process Engineering and Mechanics, Gotthard-Franz-Str. 3, 76131 Karlsruhe, Germany

We introduce a novel method to produce macroporous ceramics by capillary suspensions. Adding a small amount (1 vol%) of an immiscible secondary phase to a low concentration (20 vol%) suspension can increase the yield stress by several orders of magnitude. This drastic change in flow behavior is induced by the creation of a sample-spanning particle network in the suspension controlled by capillary forces. This strong network may persist even if the primary bulk phase is removed. Accordingly, capillary suspensions can be used as a precursor for manufacturing porous materials. Here, we focus on the specific features of this universal, low-cost processing route for porous ceramics. An Al_2O_3 model system is used to demonstrate how to adjust porosity and pore size. With this system, we were able to achieve open porosities higher than 60% with an average pore size below 10 μm.

I. Introduction

The flow behavior of suspensions can be drastically changed by adding a small amount (1 vol%) of a secondary fluid phase that is immiscible with the primary fluid phase of the suspension, and it does not matter whether the secondary fluid phase wets the particles preferentially or not.[1] The corresponding creation of a sample-spanning network is due to attractive capillary forces among particles. This is a general physical phenomenon and can be observed in many different kinds of material systems.[2] The addition of a secondary phase may reinforce an existing attractive sample-spanning network (e.g., van der Waals) or create such a network when the particles are otherwise stabilized.[3,4] The capillary force is typically much stronger than the other interparticle forces and can be used to stabilize particles in a bulk phase, tune the strength of suspensions to adjust the specific needs of certain industrial processes, or form the precursor for porous membranes, foams or macroporous ceramic materials.[5] This latter case will be discussed here in detail.

Porous materials are classified by the pore size they possess, with three different main pore size ranges[6]: microporous materials with a typical pore size <2 nm, mesoporous materials with a pore size between 2 and 50 nm and macroporous materials with pores >50 nm. In this article, we concentrate on macroporous materials. Typical process routes that are used in industry to produce macroporous ceramics are the sacrificial templating, direct foaming, replica techniques, and the partial sintering method. The respective processing steps and final sintered properties are listed in Table I. The partial sintering method is a straightforward way to produce macroporous ceramics with pores <10 μm and porosities up to 50%. After sintering, the ratio between porosity ε and pore size d_{pore} depends on the particle size of the raw ceramic powder which is used and the progress of partial sintering. This method leads to very homogenous bodies with a narrow pore size distribution.[7] The other process routes are based on the principle of introducing a negative space template into a ceramic preparation. These templates can either be a solid or a gas. After debinding and sintering, the pore represents a positive or negative counterpart to the space template. These process routes have several disadvantages when adjusting to small pores <10 μm. The replica technique and direct foaming are not suitable to meet this specification because of structural limitations of the impregnated structure or coalescence of foam bubbles. Using the sacrificial templating method to produce pores <10 μm requires the use of templating particles <10 μm and it is hard to obtain a homogenous distribution of the template particles without agglomeration.[8–11] Using the partial sintering method, a powder prepared as a suspension or compacted under pressure is sintered after debinding. Pores remain in the particle interstices because dense sintering is avoided.

The novel processing route using capillary suspensions is quite different from standard techniques mentioned above as no template or supplemental is required. Just a regular low solids ceramic suspension and a trace amount of an appropriate secondary fluid phase inducing the capillary network formation are needed. This concept leads to a controlled heterogenization of the homogeneous green suspension in which porosity and pore size can be controlled in a specific area. Open porosities well above 50% and pore sizes <10 μm can be easily achieved.

The reason for the network formation of the particles is the capillary force F_C between two or more particles linked by a capillary bridge. In Fig. 1, the main factors influencing the strength of capillary suspensions are shown for a two sphere model. The corresponding cohesion between many such particles can be described with the general rules of capillary systems in analogy to wet granular materials with a special note that the typical volume fraction in capillary suspensions is much smaller than for the close-packed granular media.[12]

Two different main states, the pendular and the capillary state are defined for capillary suspensions.[1] In the pendular state, the secondary phase preferentially wets the particles. This results in a three-phase contact angle $\theta_{S,B} < 90°$ of the suspension, where the contact angle is always defined as the angle the secondary phase (S) makes against the particles when surrounded by the bulk phase (B). There are also systems, in the capillary state, where the secondary phase does not preferentially wet the particles. The resulting $\theta_{S,B}$ is then >90°.

In this article, we focus on the pendular state, F_C can be written as[12]

$$F_C = g(\tilde{V}, \tilde{s})\Gamma_{SB}\, r \cos\theta_{S,B} \quad (1)$$

where $\Gamma_{S\ B}$ is the interfacial tension between bulk and secondary phases and r is the particle radius. The function g

A.Krell—contributing editor

Manuscript No. 31530. Received June 1, 2012; approved November 5, 2012.
†Author to whom correspondence should be addressed. e-mail: jens.dittmann@kit.edu

Table I. Typical Methods for Producing Macroporous Ceramics as well as Reached Pore Sizes d_{pore} and Porosities ε[7–11]

Method	Description	d_{pore} (μm)	ε (%)
Sacrificial templating	(1) Adding of sacrificial phase to ceramic or ceramic precursor in solid or liquid form (2) Drying, pyrolysis or evaporation to remove template (3) Sintering.	1–700	20–90
Direct foaming	(1) Gas incorporation into ceramic suspension or ceramic precursor (2) Setting or drying (3) Sintering	35–1200	40–97
Replica technique	(1) Impregnation or infiltration of a synthetic or natural template by a ceramic suspension or a ceramic precursor (2) Drying or template removal (3) Sintering	10–3000	25–95
Partial sintering	(1) Powder preparation as suspension or compacted by pressing (2) Debinding and sintering or direct sintering	<10	<50

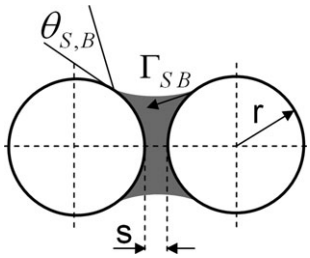

Fig. 1. Schematic drawing of a pendular drop between two spherical solid particles showing the essential parameters. The contact angle $\theta_{S,B}$ determines if the admixture is in the pendular state ($\theta_{S,B} < 90°$) or capillary state ($\theta_{S,B} > 90°$).

depends on the reduced volume of the capillary bridge $\tilde{V} = V/r^3$ and the reduced particle separation $\tilde{s} = s/r$. The van der Waals-force F_{vdW} which is always present in particle suspensions can be written as[1]

$$F_{vdW} = \frac{A_H}{12}\frac{r}{h^2} \tag{2}$$

where A_H is the Hamaker coefficient and h the distance between particle surfaces for rough particles in contact this quantity can be set equal to the average surface roughness. The three-phase contact angle $\theta_{S,B}$ is calculated using the expanded Young–Dupré equation[13–15]

$$\theta_{S,B} = \frac{\Gamma_{Sa}\cos\theta_{S,a} - \Gamma_{Ba}\cos\theta_{B,a}}{\Gamma_{SB}} \tag{3}$$

where $\Gamma_{i,a}$ is the surface tension against air (a) of the bulk and secondary phase, $\cos\theta_{i,a}$ describes the wetting angles of the respective phase against solid in air. The yield stress σ_y for $\tilde{s} = 0$ and $\tilde{V} \ll 1$ of a suspension is then given as[4,16]

$$\sigma_y = f(\phi)\frac{F_C}{r^2} = f(\phi)\, g(\tilde{V},\tilde{s})\frac{\Gamma_{SB}\cos\theta_{S,B}}{r} \tag{4}$$

where the function $f(\phi)$ depends on the number of particle–particle contacts. For sparse suspensions,[17] $f(\phi) \approx \phi^2$. Finally, the tensile stress σ_y is proportional to $\Gamma_{SB}\cos\theta_{S,B}$ and $1/r$. In addition, it increases strongly with increasing secondary volume fraction. A high yield stress is desirable for a strong precursor which does not collapse or shrink too much when the primary phase is extracted to get a highly porous ceramic material.

It is not possible to predict the yield strength or absolute values of rheological data from Eq. (4) as the number of contacts where capillary bridges are present is not known and hence the liquid volume per capillary bridge cannot be calculated. Moreover, it is not know whether the liquid bridges are all of the same size. This is ongoing research, but not decisive for the principle of the new processing route presented here.

Electrostatic interactions are not relevant for the material system investigated here, as the particles are suspended in a nonpolar solvent. Furthermore, the suspensions used in this present work are not colloidal in nature, as the particle size and the viscosity of the bulk phase are too high. Relevant here is the strength of the capillary force compared to the vdW-force acting between particles. Typical values for materials used in this present work are F_C ($\Gamma = 43.1 \times 10^{-3}$ N/m, $\theta = 66°$, $r = 10^{-6}$ m) $\approx 1.1 \times 10^{-7}$ N and F_{vdW} ($A_H = 10^{-20}$ Nm, $h = 10^{-9}$ m, $r = 10^{-6}$ m) $\approx 8.3 \times 10^{-10}$ N for a constant particle size calculated by Eq. (1) and (2). This latter force is estimated to be orders of magnitude smaller than the dominating capillary force.

II. Experimental Procedure

An overview of some solid–fluid combinations for ceramic processing with capillary suspensions is listed in Table II. Simple liquids, saturated aqueous solutions, and molten polymer materials all may be used as bulk or secondary phase. The specific material combination depends on the desired processing method and finished shape as well as the appropriate debinding steps. Here, solid bridges are preferred because of the higher stability of the particle network after bulk debinding. These solid bridges result from recrystalization of dried aqueous solutions or solidification of polymer melts. Ceramics formed from capillary suspensions are suitable for different kinds of applications and may be manufactured using paste processing with e.g., a doctor blade for thin films or injection molding to get strong, solid parts.

The processing route is demonstrated using an Al_2O_3-based system with paraffin oil as bulk phase and a saturated water–sucrose solution (1.853 M) as secondary phase. Adding the secondary fluid phase results in the formation of a paste from a freely flowing suspension of ceramic particles at room temperature.

(1) Raw Materials

The raw ceramic powder used is a calcined α-Al_2O_3 ceramic (Almatis, CT19FG, Ludwigshafen, Germany) with a volume-based particle diameter $d_{50,3}$ of 5.76 μm. The particle size analysis, Fig. 2, shows a wide distribution that is almost monomodal. The bulk phase is paraffin oil (Carl Roth, Karlsruhe, Germany) with a Newtonian flow behavior and a dynamic viscosity η of 0.03 Pa s. To get a homogenous paste without agglomerates, polysorbat 20 (Carl Roth, Tween20, Karlsruhe, Germany) was added to the bulk phase. Polysorbat 20 is a nonionic wetting agent with a hydrophilic–lipophilic balance value of 16.7. Adding this wetting agent does not change the viscosity of the bulk phase. The secondary phase used is a saturated water–sucrose solution with a concentration of 1.853 M. The sucrose is an α-D-sucrose (Carl Roth, D(+)-Sucrose, Karlsruhe, Germany) dissolved in

distilled water at room temperature. The flow behavior of the saturated solution is Newtonian with $\eta = 0.08$ Pa s.

(2) Processing Route

The main processing steps can be summarized as mixing, forming, bulk debinding, thermal debinding, and sintering. Figure. 3(a)–(d) shows the effect of each processing step on the particle network. At the beginning of the process route, there is the suspension consisting of the bulk- and solid phase [Fig. 3(a)]. After incorporating the secondary fluid phase to the homogenized suspension [Fig. 3(b)], the secondary phase forms capillary bridges between the particles and we get a homogeneous and coherent particle network in the bulk phase. The preparation step can be performed through stirring with a high shear dissolver mixer, as it was in this article, or a kneading apparatus depending on the application, material system or process equipment that is used. In the next step [Fig. 3(c)], the bulk phase is removed either by solvent extraction, capillary extraction with an absorbent pad, drying, or another convenient technique. The secondary phase works as a stabilizer to save the particle network structure after removing the bulk phase. The extraction step has to be adjusted based on the chosen material system because the bulk phase should be removed without affecting the secondary phase, leaving the particle network intact. After the bulk phase is removed, the secondary phase is pyrolyzed in a debinding oven [Fig. 3(d)]. The debinding profile should consist of a very slow heating profile to ensure that the structure does not crack. After the thermal debinding step, the ceramic powder is sintered at conditions specific to the material system.

Table II. Different Solid–Fluid Combinations of Some Material Combinations for Ceramic Processing

Solid		
Aluminum oxide, silicon dioxide, tricalcium phosphate, titanium dioxide		
	Pure	Sat. aqu. solution[†]
Bulk phase		
Paraffin oil	x	–
Paraffin wax	x	–
Decanol	x	–
Octanol	x	–
Diisononyl phthalate	x	–
Secondary phase		
Water	x	–
Sucrose	–	x
Glycerine	x	x
Polyvinyl alcohol	–	x
Polyvinyl pyrrolidone	–	x
Polyethylene glycol	x	x

[†]Sat. aqu. solution = Saturated aqueous solution

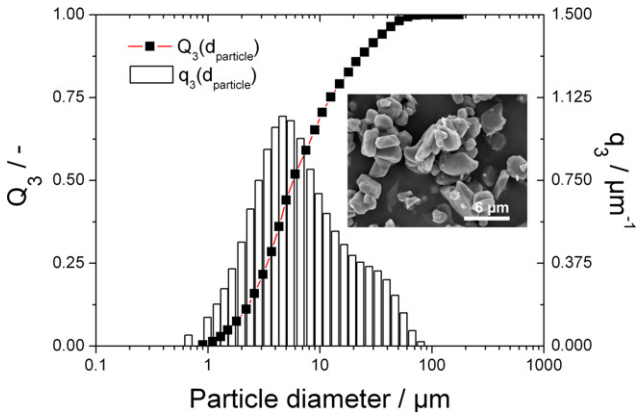

Fig. 2. Particle size analysis and SEM image of the used raw α- Al_2O_3 powder. Q_3 and q_3 are the cumulated and differential particle size distribution measured by Fraunhofer diffraction.

(A) Mixing, Forming, and Bulk Debinding: A moment-controlled high shear dissolver stirrer was used to mix the samples. The Al_2O_3 powder and the bulk phase were stirred together for 20 min at 1200 rpm at room temperature. The wetting agent was then added to the suspension and again stirred for 10 min at 1000 rpm. The surfactant controls an optimal wetting of the solid surface by the bulk phase to prevent uncontrolled reagglomeration of particles that were previously broken up by stirring with the high shear dissolver. The stirring process was monitored by a torque detector to create a homogenous, agglomerate-free suspension. The suspensions typically reached a constant torque during the initial mixing (which is assumed to correspond to a homogenous sample) after 10 min and after 1 min during the subsequent addition of the wetting agent. Particle volume fraction was varied between 15 and 25 vol%, the added wetting was 0.45 vol% relative to the bulk phase.

Following the suspension preparation, the secondary phase is added into the stirring process at 1000 rpm for 1 min before reducing the speed to 500 rpm for 1 min. Stirring the secondary phase at high speed breaks it up into small droplets such that a homogeneous distribution can be achieved for optimum wetting of the solid particles. The reduction in the mixing speed initiates the formation of the particle network in the capillary suspension. Secondary phase volume fraction was varied between 0.3 and 4 vol%. In general, the secondary phase must be liquid or molten at the mixing temperature. It may be cooled and solidified for subsequent processing steps. This admixture, a capillary suspension, is then molded into a sample form and the top face is spread with a doctor blade. Using such a mold pro-

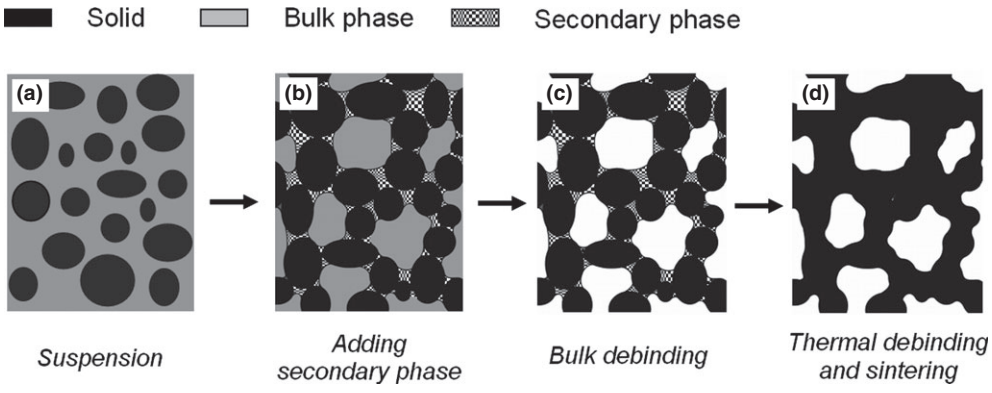

Fig. 3. Principle processing steps for the production of porous ceramics by capillary suspensions.

duces a well-defined, round sample geometry with a diameter of 2 cm and a height of 0.02 cm. The sample die is placed on an absorbent pad, the paste is spread, and then the die is removed. Through the capillaries of the absorbent pad, the majority of the bulk phase is removed from the sample in an oven at 50°C for 12 h at normal atmospheric conditions. The slight increase in temperature does not change the sample, but serves to reduce the viscosity of the bulk phase to accelerate the removal of this bulk phase. The particle network structure remains in place due to the strong capillary force from the bridges of the secondary phase between the ceramic particles after removing the sample from the oven. For the present work, crystallized sucrose crystal bridges between the particles give the sample a particularly good stability.

(B) Thermal Debinding and Sintering: After the bulk debinding step, the sample undergoes a thermal debinded step in a debinding oven at normal atmospheric conditions. The debinding profile, outlined in Fig. 4, is chosen to be conservative, allowing gentle debinding without cracking, but ensuring the organic components are completely pyrolyzed. These organic components are any remaining paraffin oil, wetting agent, and sucrose. The sample was heated up to 200°C starting from room temperature with a rate of 1°C/min and held at that temperature for 30 min. From 200°C to 500°C, the heating rate was again 1°C/min with a holding time of 70 min at 500°C. The final steps were to heat the sample to 800°C at a rate of 2.5°C/min followed by a holding time of 15 min at 800°C. Following thermal debinding, the sample was quiescently cooled to room temperature in the oven over approximately 180 min. The sintering profile, also outlined at Fig. 4, begins at room temperature with a heating rate of 3°C/min up to 200°C and then direct heating up to 1650°C at 5°C/min where the sample was held for 120 min at normal atmospheric conditions. Following sintering, the sample was cooled down to room temperature over approximately 300 min.

(3) Characterization

The initial particle size distribution was measured through Fraunhofer diffraction (Sympatec, Helos H0309, Clausthal-Zellerfeld, Germany) with a wet dispersing unit (Sympatec, Quixel, Clausthal-Zellerfeld, Germany). For the rheological characterization, a shear rheometer (Thermo Scientific, Mars II, Karlsruhe, Germany) was used with a cone/plate (CP 60/1) and plate/ plate (PP35) geometry for the viscosity measurements. The yield stress was measured using a vane geometry (Z20 according to DIN 53019-1) on the same rheometer and evaluated by the tangent method.[18] In both cases, the measurements were carried out using shear stress ramps. The surface and interfacial tension was determined using a weight-based tensiometer (Dataphysics, DCAT 11, Filderstadt, Germany) employing a Wilhelmy plate. The contact angle was measured through the sessile drop method (Dataphysics, OCA15, Filderstadt, Germany) and evaluated by a numerical Young-Laplace fit.[19] The porosity was measured by determining the Archimedes density according to DIN EN 993-1. Mercury porosimetry was used to determine the pore size distribution (Micromeritics, Auto Pore III, Aachen, Germany). The samples were vacuum infused with epoxy resin, mounting on SiC paper and polished with a diamond suspension (Buehler, Düsseldorf, Germany) for crosscut scanning electron microscopy (SEM) images. Crosscut SEM images were taken in backscattering-mode and fracture area images in secondary electron mode (Hitachi, S-4500, Krefeld, Germany).

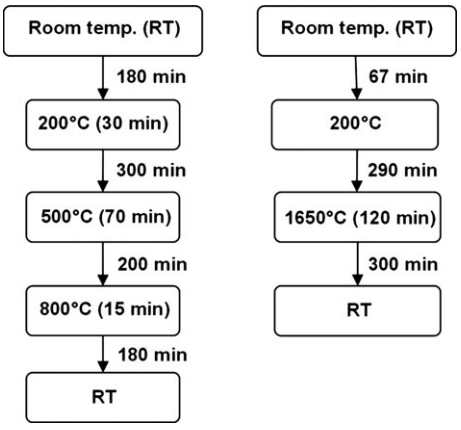

Fig. 4. Thermal debinding (left) and sintering profile (right) used in the production of porous ceramics from a capillary suspension following the bulk debinding step.

III. Results and Discussion

The stability of the capillary suspension is controlled by the strength of the interface and in particular by the interfacial tension $\Gamma_{S\ B}$ and the contact angle $\theta_{S,B}$. High interfacial tensions result in a stable capillary system without phase separation as, according to Eq. (3), the yield stress σ_y increases linearly with $\Gamma_{S\ B}$. The water–sucrose solution has a surface tension of 77.5 mN/m and a contact angle against air on Al_2O_3 of 51.8°. Paraffin oil has a surface tension of 30.4 mN/m and a contact angle of 0° against air on Al_2O_3, this means complete wetting. Combining the water–sucrose solution together with paraffin oil as bulk phase results in an interfacial tension Γ_{12} of 43.1 mN/m. These factors determine the three-phase contact angle in the capillary suspension, which is calculated as 66°, a value in the pendular state.

(1) Rheological Characterization

The macroscopic texture of capillary Al_2O_3 suspensions with a constant volume fraction of $\phi = 20$ vol% is displayed at Fig. 5. The increase in gel strength and the corresponding change in texture upon addition of trace amounts of the secondary phase are clearly evident. This demonstrates the formation of a sample-spanning particle network, which is used to produce macroporous ceramic materials.

Yield stress data for capillary suspension including the wetting agent are shown in [Fig. 6(a)]. The resulting yield stress σ_y is plotted as a function of the fraction of secondary phase, with respect to the total fluid volume, for several particle volume fractions ϕ. The system demonstrates the typical behavior of a capillary suspension: the measured yield stress increases by at least one order of magnitude when adding an increasing amount of secondary phase to the suspension. Similar results have been obtained for various other systems.[1–4] For secondary phase amounts greater than 1 vol%, a plateau value for the yield stress is reached. This plateau demonstrates a saturation of the capillary suspension. In this case, saturation means that almost all of the contact points between the particles now contain bridges of secondary phase and a coherent network is formed where subsequent second-

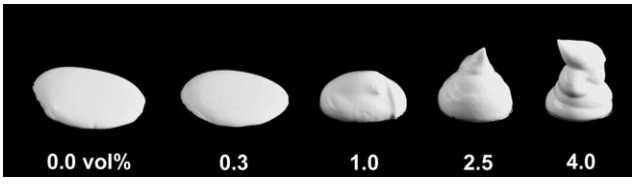

Fig. 5. Characteristic texture of Al_2O_3 powder (ϕ = const. = 20 vol%) in paraffin oil with different amounts of secondary phase (H_2O–sucrose solution, 1.853 M).

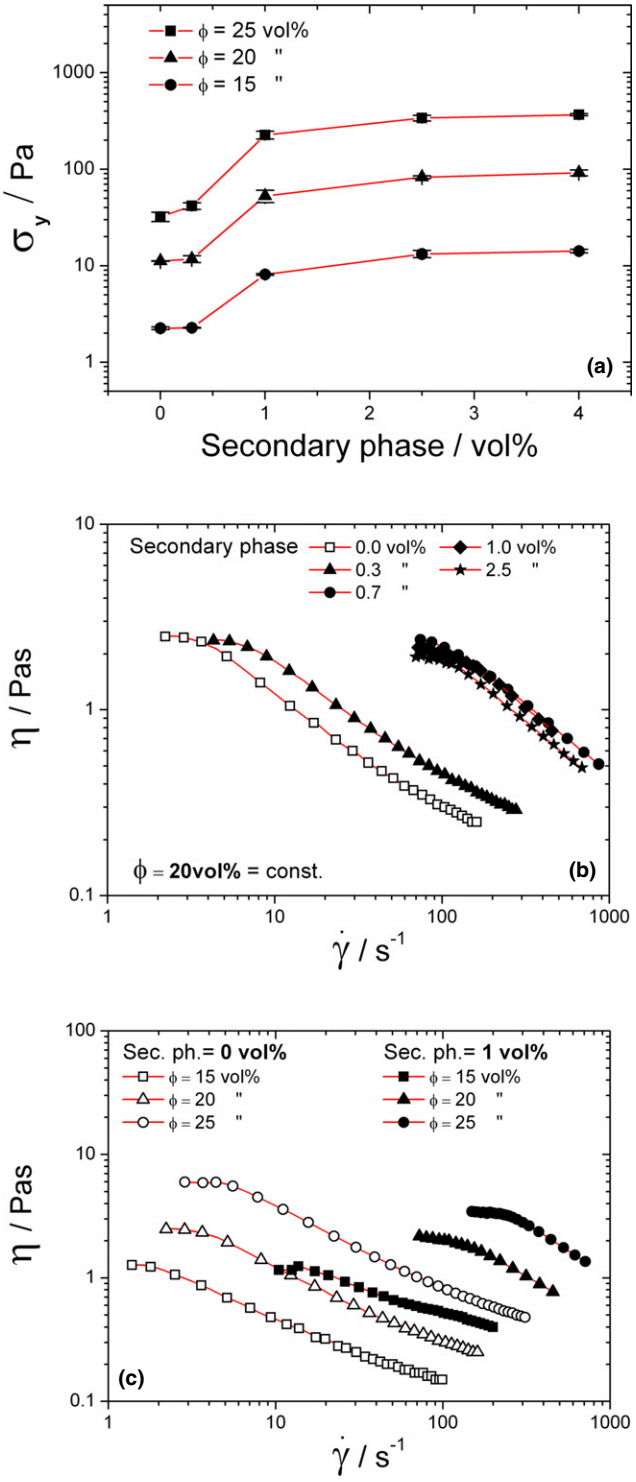

Fig. 6. Yield stress data (a) and viscosity curves (b, c) for varying solid fractions and different fractions of secondary phase.

ary phase no longer drastically influences the network strength. For values greater than 4 vol%, no further increase in yield stress is observed because the particle network is saturated. Capillary suspensions show a typical shear thinning behavior, as shown in [Fig. 6(a) and (c)], where the viscosity η is plotted as a function of the shear rate $\dot{\gamma}$. Increasing the amount of secondary phase results in a shift of the viscosity curves to higher shear rates. As with the yield stress, a maximum shift is reached and the curves begin to overlap as demonstrated in Fig. 6(b) for $\phi = 20$ vol% when a critical value of secondary phase fraction is reached. As shown in Fig. 6(c), this characteristic shifting of η to higher shear rates

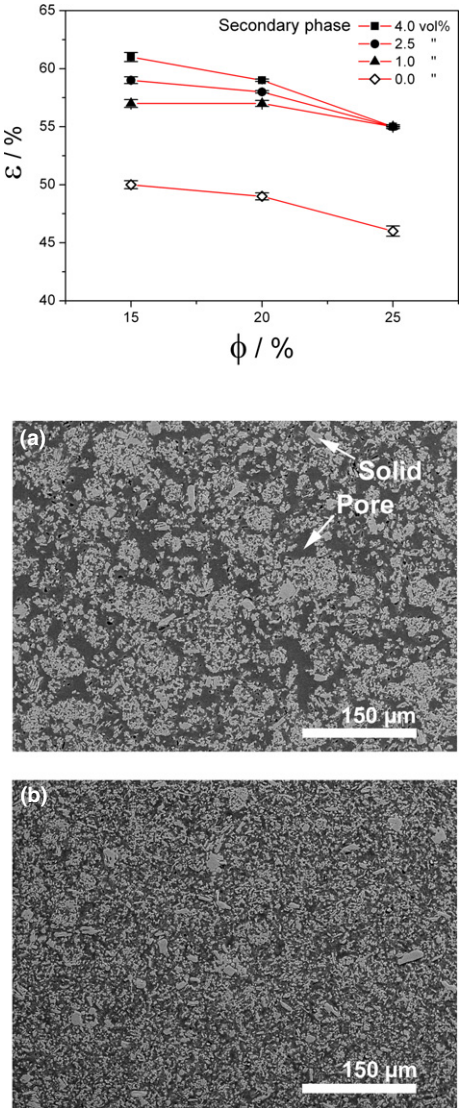

Fig. 7. Variation of porosity ε with particle concentration ϕ for several amounts of secondary phase. The error bars are the standard deviations calculated from at least three measurements. SEM crosscut images at points (a) ($\phi = 15$ vol%, 4.0 vol% secondary phase) and (b) ($\phi = 25$ vol%, no secondary phase). Solid Al_2O_3 particles appear light gray and pores as dark gray in these images.

is confirmed for constant amounts of secondary phase and different ϕ. Variations of particle loading roughly result in a shift of the flow curves along the first bisector in the log-log plot of η versus $\dot{\gamma}$ with and also without secondary phase as shown in Fig. 6(c).

The rheological data presented in Fig. 6 demonstrate the effect of the capillary force on suspension rheology. The major impact here is the creation of the particle network by adding the secondary phase to a pure suspension from which the porosity of the sintered part results. This change in the rheological behavior proves the structure creation already in the wet state of the pastes which then is observed in the sintered parts in a very clear way. Furthermore, the rheological data will be important for the layout of the processing equipment if such suspensions are processed on a technical scale.

(2) Porosity

The porosity was the principal criterion for characterizing the sintered parts. The porosity curves, Fig. 7, show the same dependence on the secondary phase and volume fraction as

the yield stress measurements [Fig. 6(a)]. In Fig. 7, the porosity ε is plotted as a function of particle volume fraction for different concentrations of secondary phase. In all cases, the porosity is significantly higher for the capillary suspension than for the corresponding suspensions without secondary phase which represents the partial sintering method. For the $\phi = 15$ vol% suspensions, the porosity monotonically increases with increasing secondary phase content, but this effect decreases with increasing ϕ. As expected, the porosity decreases since ϕ increases for capillary as well as regular suspensions. These results indicate that the particle network in the capillary suspensions is stable and neither settling nor phase separation are present. The final porosity comes from the structures created by the capillary force in these suspensions. The porosity of the sintered parts, as formed by capillary suspensions, is completely open without closed pores. The capillary effect offers an additional degree of freedom in determining the porosity of ceramic materials. In addition, this gives access to unusually high open porosities, which are advantageous in various industrial applications including manufacturing of ceramic filters. The different structures created by capillary suspensions compared with regular suspensions can directly be seen in the crosscut images of the corresponding sintered ceramics shown in Fig. 7 (a) and (b). Here, the controlled heterogenization of the homogenous green suspensions is clearly visible. The porosity of the sintered parts, as formed by capillary suspensions, is completely open without closed pores. Obviously, the capillary effect not only increases the porosity but also broadens the pore size distribution. This will be discussed in more detail in the next section.

(3) Pore Size and Structure Characteristics

Pore shape and pore size are changed due to the capillary effect as can be seen from the images shown in Fig. 7 (a) and (b). The change in pore size distribution due to the added secondary phase fraction has been quantitatively analyzed using mercury porosimetry. Corresponding data for suspensions with $\phi = 15$ vol% are shown in Fig. 8. Adding 2.5 vol% secondary phase to the suspension increases the average pore size from about 2 to 5.5 μm but essentially retains the monomodal size distribution. Further increasing the secondary phase fraction to 4 vol% (where σ_y becomes constant) increases the pore size slightly and the size distribution clearly becomes wider. This demonstrates that by increasing the amount of secondary phase into the saturated region leads to a multimodal pore size distribution.

The broadening of the pore size distribution in sintered ceramic parts made from capillary suspensions is due to the formation of flocs from individual primary particles, which in turn is attributed to the capillary bridges formed by the secondary phase. This floc structure is easily seen in the fracture area images shown in Fig. 9. Increasing the amount of secondary phase at a constant ϕ causes the flocs to grow with the creation of a staggered, multimodal pore size distribution. For these systems, small pores are internal to the flocs and larger pores formed from the areas between where the flocs are superordinated. The measured pore size characteristic is confirmed by the optical impression. In general, decreasing ϕ and increasing the amount of secondary phase results in an increase in pore size and finally the pore diameter increases with increasing porosity as shown in Fig. 10.

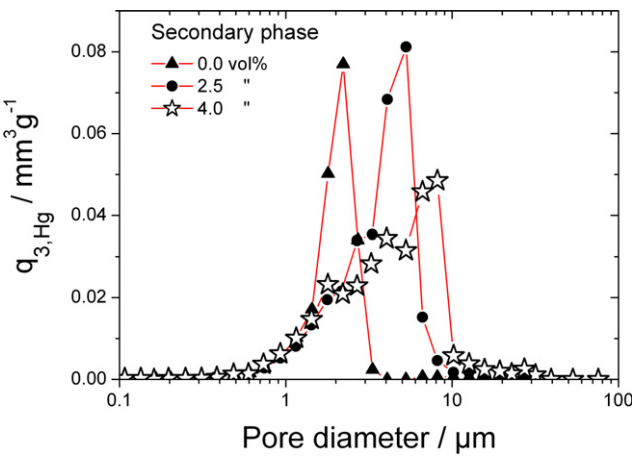

Fig. 8. Pore size distributions of sintered parts for several amounts of secondary phase at a constant value of solid $\phi = 15$ vol%. $q_{3,Hg}$ is the differential pore size distribution determined by mercury porosimetry.

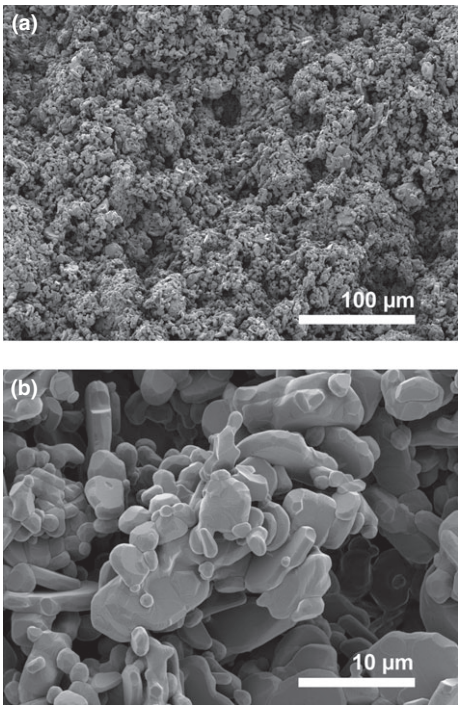

Fig. 9. SEM fracture area images following sintering showing floc creation by adding secondary phase to a suspension.

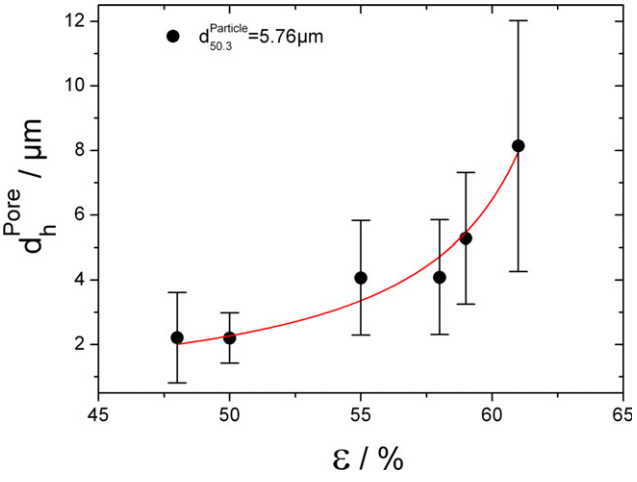

Fig. 10. Correlation between the mode (most frequent value) of pore size d_h^{Pore} as a function of the porosity ε. The error bars are the standard deviations calculated using the x_{10}, x_{50}, and x_{90} values of the pore size distribution $q_{3,Hg}$ obtained from mercury porosimetry. x_i denotes the size value for which i percent is smaller than this value.

IV. Conclusions

In this article, we introduced a novel processing route for the manufacturing of macroporous ceramics. The new concept is based on improving the approach of partial sintering by a controlled heterogenization of homogeneous green suspensions. This makes the new concept widely applicable as low cost route for macroporous ceramics relying only on processing operations that are well established in ceramics industry and it gives access to porous materials with pore sizes less than 10 μm and porosities well above 50%. The key step is to prepare a capillary suspension of the respective ceramic powder. In such suspensions, capillary forces are used to create flocculated particle networks in the bulk phase of the suspension through adding a secondary fluid phase. The strong particle network formed by capillary suspensions yields a high open porosity without a conventional volume displacer. The use of capillary suspensions for the creation of porous ceramics simplifies the processing of these materials and is potentially able to do so with less waste and at significant cost savings.

The resulting structure of the sintered part can be adjusted through the choice of material combinations. Changing the volume fraction of solid or the amount of secondary phase has a direct influence on the pore characteristic in the sintered part. For constant particle size and volume fraction of solids, increasing the amount of secondary phase results in an increase in the pore size and porosity. Furthermore, a transition from a sharp monomodular pore characteristic to a wider and staggered multimodal pore structure occurs at higher secondary phase contents. The high open porosities, where closed pores are nonexistent, are interesting for applications where high inner surfaces for mass transfer or permeability are important, e.g., precursors for catalytic carriers or filter membranes. The advantage of the novel processing route is that the resulting pore structure is adjusted during preparation by the mixing of the ceramic powder into self-organizing network.

The novel process route using capillary suspensions has the potential to cover a wide range of porosities and pore sizes using different combinations of particle sizes, amounts of solid fractions, and secondary phases. The route can also be combined with conventional methods so that these routes can be optimized in porosity and pore size. Furthermore, capillary forces can be used for tuning the rheology of ceramic suspensions in a wide range with the addition of an appropriate secondary phase. This concept is a versatile means to adjust the flow properties according to the demand of different processing techniques. In particular sedimentation and phase separation can be easily avoided through the resulting network formation.

V. Outlook

Ongoing research will focus on the elucidation of structure formation and the investigation of the mechanical stability of sintered porous ceramic membranes made from capillary suspensions. Using high-resolution X-ray tomography for 3-D reconstruction and image analysis from SEM crosscut images will allow a quantitative characterization of the microstructure and the kinetics of the structure buildup. Especially for industrial applications the mechanical stability of the final sintered parts is important. It is well-known that for homogenous sintered bodies the mechanical stability depends only on porosity, but not on the pore size.[20] This behavior changes if the pore structure consists mainly of interconnected pores[21] which is the dominant pore structure characteristic of sintered capillary suspensions. Because of the controlled heterogenization of homogenous green suspensions, it is expected that for a constant fraction of solid and an increasing amount of secondary phase the resulting increase in porosity and pore size leads to a decrease in the mechanical stability. An accurate experimental characterization and the comparison with existing models is dedicated to further research.

Acknowledgments

We would like to thank the DFG for funding (grant no. Wi 3138/6-1). Further thanks are given to Almatis GmbH for the donation of the alumina powder. Thanks to Thomas Lebe for the work at the SEM microscope and Boris Bitsch for contributing to the rheological measurements. We would also like to thank the Institute for Applied Materials (KIT), especially Günther Schell and Claudia Bucharsky, for interesting discussions and support in sintering the ceramics.

References

[1]E. Koos and N. Willenbacher, "Capillary Forces in Suspension Rheology," *Science*, **331**, 897–900 (2011).

[2]E. Koos, J. Dittmann, and N. Willenbacher, "Capillary Forces in Suspensions: Rheological Properties and Potential Applications", "Kapillarkräfte in Suspensionen: Rheologische Eigenschaften und Potentielle Anwendungen", *Chem. Ing. Tech.*, **83** [8] 1305–9 (2011).

[3]E. Koos and N. Willenbacher, "Particle Configurations and Gelation in Capillary Suspensions," *Soft Matter*, **8**, 3988–94 (2012).

[4]E. Koos, J. Johannsmeier, L. Schwebler, and N. Willenbacher, "Tuning Suspension Rheology Using Capillary Forces," *Soft Matter*, **8**, 6620–8 (2012).

[5]J. Dittmann, E. Koos, N. Willenbacher, and B. Hochstein, "Process Route Fort the Production of a Porous Ceramic and Thereby Available Porous Ceramic", "Verfahren zur Herstellung Einer Porösen Keramik und Damit Erhältliche Poröse Keramik"; German Patent DE 10 2011 106 834.5, 2011.

[6]K. Ishizaki, S. Komarneni, and M. Nanko, *Porous Materials*. Kluwer Academic Publishers, Dordrecht, 1998.

[7]T. Ohji and M. Fukushima, "Macro-Porous Ceramics: Processing and Properties," *Int. Mater. Rev.*, **52** [2] 115–31 (2012).

[8]S. Woyansky, C. E. Scott, and W. P. Minnear, "Processing of Porous Ceramics," *Am. Ceram. Soc. Bull.*, **71** [11] 1674–82 (1992).

[9]L. Montanaro, Y. Jorand, G. Fantozzi, and A. Negro, "Ceramic Foams by Powder Processing," *J. Eur. Ceram. Soc.*, **18**, 1339–50 (1998).

[10]S. H. Li, J. R. Wijn, P. Layrolle, and K. Groot, "Novel Method to Manufacture Porous Hydroxyapatite by Dual-Phase Mixing," *J. Am. Ceram. Soc.*, **86** [1] 65–72 (2003).

[11]A. R. Studart, U. T. Gonzenbach, E. Tervoort, and L. J. Gaukler, "Processing Routes to Macroporous Ceramics: A Review," *J. Am. Ceram. Soc.*, **89** [6] 1771–89 (2006).

[12]H. Schubert, *Capillarity in Porous Solid Systems, Kapillarität in Porösen Feststoffsystemen*. Springer Verlag, Berlin, 1982.

[13]B. P. Binks and J. H. Clint, "Solid Wettability From Surface Energy Components: Relevance to Pickering Emulsions," *Langmuir*, **18**, 1270–3 (2002).

[14]R. Aveyard, B. P. Binks, and J. H. Clint, "Emulsions Stabilized Solely by Colloidal Particles," *Adv. Colloid Interface Sci.*, **100–102**, 503–46 (2003).

[15]C. O. Fournier, L. Fradette, and P. A. Tanguy, "Effect of Dispersed Phase Viscosity on Solid-Stabilized Emulsions," *Chem. Eng. Res. Des.*, **87**, 499–506 (2009).

[16]H. Schubert, "Capillary Forces – Modeling and Application in Particulate Technology," *Powder Technol.*, **37**, 105–16 (1984).

[17]W. B. Pietsch and H. Rumpf, "Strength, Capillary Pressure, Fluid Volume and Cross Angle Between two Spheres", "Haftkraft, Kapillardruck, Flüssigkeitsvolumen und Grenzwinkel Einer Flüssigkeitsbrücke Zwischen Zwei Kugeln," *Chem. Ing. Tech.*, **39**, 885–93 (1967).

[18]Q. D. Nguyen and D. V. Boger, "Measuring the Flow Properties of Yield Stress Fluids," *Annu. Rev. Fluid Mech.*, **24**, 47–88 (1992).

[19]M. Bartolotti, M. Brugnara, C. D. Volpe, and S. Siboni, "Numerical Models for the Evaluation of the Contact Angle From Axisymmetricdrop Profiles: A Statistical Comparison," *J. Colloid Interface Sci.*, **336**, 285–97 (2009).

[20]Y. B. P. Kwan, D. J. Stephenson, and J. R. Alcock, "The Porosity Dependence of Flexural Modulus and Strength for Capsule-Free hot Isostatically Pressed Porous Alumina," *J. Mater. Sci.*, **35** [5] 1205–11 (2000).

[21]D. Hardy and D. J. Green, "Mechanical Properties of a Partially Sintered Alumina," *J. Eur. Ceram. Soc*, **15** [8] 769–75 (1995). □